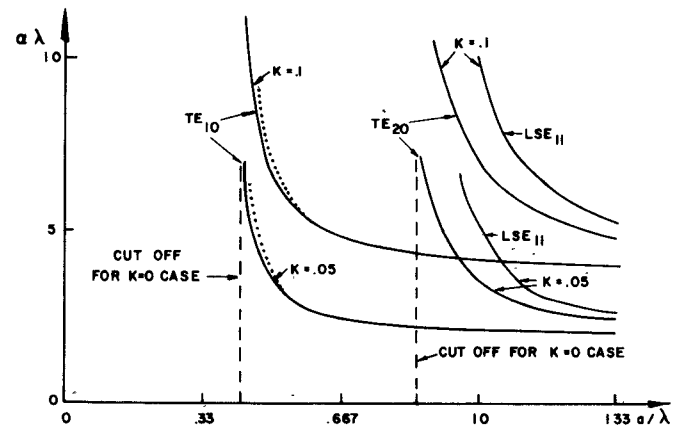

Fig. 2. Dispersion curves for an inhomogeneous lossy dielectric where K is defined by $K = \epsilon''/\epsilon'$. The dotted line represents dispersion curves for the homogeneous loading of average permittivity when $K = 0.1$.

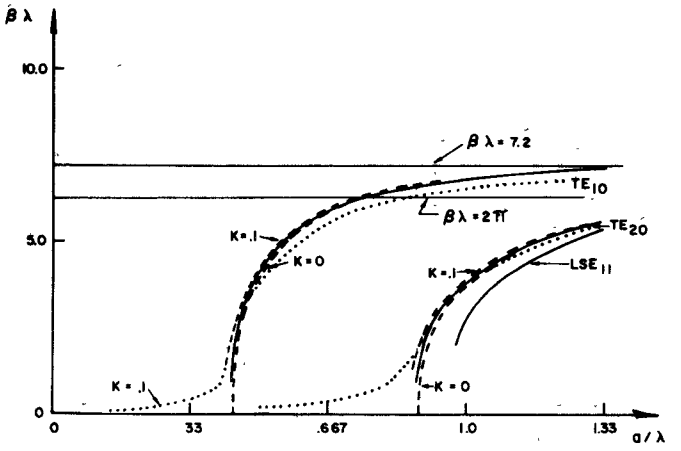

Fig. 3. Loss curves for an inhomogeneous lossy dielectric TE_{10} mode, TE_{20} mode, and LSE_{11} mode. Comparison is made with a homogeneous lossy dielectric (dotted line) for the TE_{10} mode.

with waveguides containing solid-state materials whose dielectric properties vary over distances which cannot be neglected compared to a wavelength. However, for those problems where the dielectric material is accurately modeled by a small number of dielectric slabs, our method is cumbersome owing to the step discontinuities. In those cases, the reader is advised to follow one of the referenced procedures.

REFERENCES

[1] R. E. Collins, *Field Theory of Guided Waves*. New York: McGraw-Hill, 1960.
[2] R. Seckelmann, "Propagation of TE modes in dielectric loaded waveguides," *IEEE Trans. Microwave Theory Tech.*, vol. MTT-14, pp. 518–527, Nov. 1966.
[3] N. Eberhardt, "Propagation on the off center E-plane dielectrically loaded waveguide," *IEEE Trans. Microwave Theory Tech.*, vol. MTT-15, pp. 282–289, May 1967.
[4] G. N. Tsandoulas, D. H. Temme, and F. G. Willwerth, "Longitudinal section mode analysis of dielectrically loaded rectangular waveguides with application to phase shifter design," *IEEE Trans. Microwave Theory Tech.*, vol. MTT-18, pp. 88–95, Feb. 1970.
[5] D. T. Thomas, "Functional approximations for solving boundary value problems by computer," *IEEE Trans. Microwave Theory Tech. (Special Issue in Computer-Oriented Microwave Practices)*, vol. MTT-17, pp. 447–453, Aug. 1969.
[6] W. Baier, "Wave and evanescent fields in rectangular waveguides filled with a transversely inhomogeneous dielectric," *IEEE Trans. Microwave Theory Tech.*, vol. MTT-18, pp. 696–705, Oct. 1970.
[7] W. E. Hord, and F. J. Rosenbaum, "Approximation technique for dielectric loaded waveguides," *IEEE Trans. Microwave Theory Tech.*, vol. MTT-16, pp. 228–233, Apr. 1968.
[8] A. S. Vander Vorst, A. A. Laloux, and R. J. M. Govaerts, "A computer optimization of the Rayleigh-Ritz method," *IEEE Trans. Microwave Theory Tech. (Special Issue on Computer-Oriented Microwave Practices)*, vol. MTT-17, pp. 454–460, Aug. 1969.
[9] M. J. Beaubien and A. Wexler, "An accurate finite-difference method for higher order waveguide modes," *IEEE Trans. Microwave Theory Tech. (1968 Symposium Issue)*, vol. MTT-16, pp. 1007–1017, Dec. 1968.
[10] S. Ahmed and P. Daly, "Finite element methods for inhomogeneous waveguides," *Proc. Inst. Elec. Eng.*, vol. 116, pp. 970–973, Oct. 1969.
[11] Z. J. Csendes and P. Silvester, "Numerical solution of dielectric loaded waveguides: I—Finite-element analysis," *IEEE Trans. Microwave Theory Tech. (1970 Symposium Issue)*, vol. MTT-18, pp. 1124–1131, Dec. 1970.
[12] ——, "Numerical solution of dielectric loaded waveguides: II—Modal approximation technique," *IEEE Trans. Microwave Theory Tech.*, vol. MTT-19, pp. 504–509, June 1971.
[13] H. R. Witt, R. E. Biss, and E. L. Price, "Propagation constants of a waveguide containing parallel sheets of finite conductivity," *IEEE Trans. Microwave Theory Tech.*, vol. MTT-15, pp. 232–239, Apr. 1967.
[14] W. J. English, "A computer-implemented vector variational solution of loaded rectangular waveguides," *SIAM J. Appl. Math.*, vol. 21, pp. 461–468, Nov. 1971.
[15] R. E. McIntosh and L. J. Turgeon, "Propagation along transversely inhomogeneous coaxial transmission lines," *IEEE Trans. Microwave Theory Tech.* (Short Papers), vol. MTT-21, pp. 139–142, Mar. 1973.
[16] P. H. Vartanian, W. P. Ayres, and A. L. Helgesson, "Propagation in dielectric slab loaded rectangular waveguide," *IRE Trans. Microwave Tech.*, vol. MTT-6, pp. 215–222, Apr. 1958.
[17] F. E. Gardiol, "Higher-order modes in dielectrically loaded rectangular waveguides," *IEEE Trans. Microwave Theory Tech.*, vol. MTT-16, pp. 919–924, Nov. 1968.
[18] ——, "Anisotropic slabs in rectangular waveguides," *IEEE Trans. Microwave Theory Tech.*, vol. MTT-18, pp. 461–467, Aug. 1970.
[19] A. Ralston and H. S. Wilf, *Mathematical Methods for Digital Computers*. New York: Wiley, 1960, p. 100 and p. 115.
[20] R. F. Harrington, *Time-Harmonic Electromagnetic Fields*. New York: McGraw-Hill, 1961.

Operation Modes of a Waveguide Y Circulator

YOSHIHIKO AKAIWA

***Abstract*—Operation modes of a waveguide Y circulator with a circular and a triangular ferrite post are investigated both theoretically and experimentally. Field analysis is carried out taking into consideration the field variation along the ferrite axis. Frequencies are calculated by assuming TM modes nearly agree with measured frequencies. It is shown that the circulator action occurs at frequencies where two HE modes interfere with each other, besides occurring at HE mode resonance frequencies. Effects of Teflon spacers on circulator performances are investigated in detail.**

I. INTRODUCTION

The waveguide Y circulator has been widely used in microwave circuits since the first introduction by Chait and Curry [1] in 1959. The design concepts are based on the general theory of the scattering matrix established by Auld [2] and on theories of field analyses by Bosma [3] and Fay and Comstock [4]. These theories are not sufficient, since the scattering matrix theory never shows internal fields of the circulator and the field analysis theory is for stripline circulators.

Determination of operation modes is most important for circulator design, since the circulation occurs at the mode resonance frequencies. Surface wave modes had been considered by Skomal [5] to explain the circulation, however, experiments were not carried out to assert the surfaces wave modes. Little has been known about the waveguide circulator modes for a long time. Recently, Owen [6] first clarified the operation modes of a waveguide Y circulator by measuring the eigenvalues. He showed for partial height ferrites that fields vary along the axis of the ferrite and clearly showed that circulator operation is obtained at the resonance frequencies of the ferrite for rotational phase eigen excitations. He identified the ferrite resonance modes as HE_{mnl} modes. The fact that the fields vary along the axis of ferrite has not been taken into consideration in waveguide circulator theories developed before [7], [8].

Although field analysis was carried out taking into consideration the variation along the ferrite post axis for a demagnetized ferrite post, the ferrite resonance phenomena was not recognized to be important for circulator operation and the operation modes were not discussed [9].

Manuscript received November 12, 1973; revised July 15, 1974.
The author is with the Central Research Laboratories, Nippon Electric Company, Ltd., Kawasaki, Japan.

This short paper reports both theoretical and experimental investigations of waveguide Y-circulator operation modes. Field analysis is carried out for a circular and a triangular ferrite post taking into consideration the field variation along the ferrite post axis. Operation modes are investigated experimentally by measuring transmission losses, input impedance, and eigenvalues as a function of frequency. Measured resonance frequencies are compared with the calculated frequencies. Effects of a Teflon spacer on circulator performances are investigated in detail.

II. FIELDS AND RESONANCE FREQUENCY OF A CIRCULAR FERRITE POST

TM modes with respect to the axis of a circular ferrite post are assumed, since we are considering the H-plane Y-junction circulators. Coordinates are shown in Fig. 1. Assuming the fields are expressed as follows:

$$\psi = P(r) \exp [j(k_l z + m\phi - \omega t)] \tag{1}$$

the following equation is given for the Z component of the electric field:

$$\frac{\partial^2 E_z}{\partial r^2} + \frac{1}{r}\frac{\partial E_z}{\partial r} + \left[\omega\epsilon \frac{(\omega\mu - k_l^2/\omega\epsilon)^2 - (\omega\kappa)^2}{\omega\mu - k_l^2/\omega\epsilon} - \left(\frac{m}{r}\right)^2\right] E_z = 0 \tag{2}$$

where μ and κ are the components of the tensor permeability $\tilde{\mu}$:

$$\tilde{\mu} = \begin{pmatrix} u & -j\kappa & 0 \\ j\kappa & \mu & 0 \\ 0 & 0 & 1 \end{pmatrix}. \tag{3}$$

When the ferrite anisotropy is small, i.e., $\kappa/\mu \ll 1$, (2) is approximated as follows:

$$\frac{\partial^2 E_z}{\partial r^2} + \frac{1}{r}\frac{\partial E_z}{\partial r} + \left\{k'^2 - \left(\frac{m}{r}\right)^2\right\} E_z = 0 \tag{4}$$

where

$$k'^2 = \omega^2\epsilon\mu - k_l^2. \tag{5}$$

Fields are given as follows:

$$E_z \doteqdot \sum_{-\infty}^{\infty} A_m J_m(k'r) \exp [j(k_l z + m\phi)] \tag{6}$$

$$H_r \doteqdot -\frac{\omega\epsilon}{k'} \sum_{-\infty}^{\infty} A_m \left\{\frac{\omega^2\epsilon\kappa}{k'^2} J_m'(k'r) - \frac{m}{k'r} J_m(k'r)\right\} \exp [j(k_l z + m\phi)] \tag{7}$$

$$H_\phi \doteqdot j\frac{\omega\epsilon}{k'} \sum_{-\infty}^{\infty} A_m \left\{J_{m-1}(k'r) - \left(1 + \frac{\kappa}{\mu}\frac{\omega^2\epsilon\mu}{k'^2}\right)\frac{m}{k'r} J_m(k'r)\right\} \cdot \exp [j(k_l z + m\phi)] \tag{8}$$

$$H_z = 0 \tag{9}$$

$$E_r = \frac{k_l}{\omega\epsilon} H_\phi \tag{10}$$

$$E_\phi = -\frac{k_l}{\omega\epsilon} H_r \tag{11}$$

where $J_m(x)$ is the Bessel function of order m. It is assumed that the ferrite is open circuited at the side wall, since the relative dielectric constant is much larger than unity. Then the tangential components should vanish at the wall, i.e., $H_\phi = 0$ at $r = R$. It can be easily shown that resonance frequencies for two rotational phase eigen excitations, are split because of the existence of κ/μ in (8). Also, bottom and top surfaces of the ferrite post are assumed to be short or open circuited. The propagation constant k_l is given as follows:

$$k_l = (l/L)\pi \tag{12}$$

where L is the length of the ferrite and l is given as follows:

$$l = 0,1,2,\cdots \quad \text{(both surfaces are short circuited)} \tag{13}$$

$$l = 1,2,3,\cdots \quad \text{(both surfaces are open circuited)} \tag{14}$$

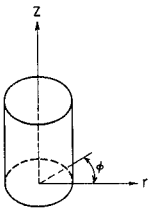

Fig. 1. Coordinates for a circular ferrites post.

$$l = 0.5,1.5,2.5,\cdots \quad \text{(one surface is open circuited and another is short circuited)}. \tag{15}$$

When the ferrite is demagnetized ($\kappa/\mu = 0$), the resonance frequencies for rotational phase eigen excitations are degenerate and can be obtained as follows:

$$f = \frac{\omega}{2\pi} = \frac{[x_{mn}^2 + (R/Ll\pi)^2]^{1/2}}{2\pi(\epsilon\mu)^{1/2}R} \tag{16}$$

where x_{mn} is the nth root of $Jm'(x) = 0$. The integer m does not take the value of zero or the value of multiples of three owing to the field symmetry for the rotational phase eigen excitations.

Resonance modes are designated $TM_{mnl}^{z_1,z_2}$ where Z_1 and Z_2 represent the impedance at the bottom and top surfaces, respectively. For example, $TM_{mnl}^{0\infty}$ indicates that the bottom surface is short circuited and the top surface is open circuited.

When the ferrite boundary surfaces are not completely open circuited, fields exist outside of the ferrite post. In this case, the boundary conditions that tangential components should be continuous at the side wall, are satisfied only when $k_l = 0$ if the ferrite post is magnetized, and when $k_l = 0$ or $m = 0$ if the ferrite post is demagnetized. For the other modes, TM modes themselves cannot satisfy the boundary conditions and hybrid modes which have both E_z and H_z should be employed. However, it can be considered that the hybrid mode fields are not so very different from the TM mode fields, since the ferrite dielectric constant is much larger than unity. Therefore, calculated TM mode frequencies assuming perfect open boundary may not be very different from measured frequencies. For the cases $k_l = 0$ or $m = 0$, the boundary conditions are reduced to the following equations [10], [11]:

$$\frac{\epsilon}{k_i R}\frac{J_m'(k_i R)}{J_m(k_i R)} = \frac{\epsilon_o}{k_o R}\frac{H_m^{(2)\prime}(k_o R)}{H_m^{(2)}(k_o R)} \tag{17}$$

where k_i and k_o are radial propagation constants inside and outside the ferrite post, respectively, and are given as follows:

$$k_i = (\omega^2\epsilon\mu - k_l^2)^{1/2} \tag{18}$$

$$k_o = (\omega^2\epsilon_o\mu - k_l^2)^{1/2}. \tag{19}$$

The open boundary conditions at the bottom or top surface can not be satisfied for any TM modes if the ferrite post is magnetized and can be satisfied for any TM modes if the ferrite post is demagnetized. For the demagnetized ferrite post, the conditions are reduced to the following equation [12]:

$$(k_l/\epsilon) \tan (k_l L) = -(k_{lo}/\epsilon_o) \tan [k_{lo}(b - L)] \tag{20}$$

where b is the height of the waveguide, k_l and k_{lo} are the longitudinal propagation constants inside and outside the ferrite post, respectively, and are given as follows:

$$k_l = (\omega^2\epsilon\mu - k_i^2)^{1/2} \tag{21}$$

$$k_{lo} = (\omega^2\epsilon_o\mu - k_i^2)^{1/2}. \tag{22}$$

It is useful to note that the resonance modes, for example HE_{111}^{00}, having symmetrical fields with respect to the plane which cuts the Y junction horizontally just at the middle point of the waveguide height, can not be excited, since the waveguide TE_{10} mode has antisymmetric fields with respect to the previously described horizontal plane. When that symmetry of a waveguide Y junction is not perfect, the symmetric resonance modes can be excited and often appear near the operation modes. For example, HE_{111}^{00} mode appears near $HE_{111}^{\infty\infty}$ modes. The former is effectively excluded by inserting a metal plate at the middle of the ferrite post.

III. EXPERIMENTS

A Y junction is made of X-band waveguides whose inside dimensions are 11.43 × 22.86 mm, considering the application to other frequency bands in which waveguide inside dimensions have the ratio of 1:2. Broad-band matching sections are introduced to match the measuring waveguide system which has 10.16- × 22.86-mm dimensions. For the convenience of loading a ferrite post, thin plates (15-mm diam × 0.3 mm thick) are mounted at the top and bottom of the center of the Y junction. A ferrite post is mounted on the plate with epoxy resin.

Fig. 2 shows transmission losses. Forward and backward losses are measured by reversing the polarity of the applied field. There are three operating regions in a waveguide band. The direction of circulation at the middle region is opposite to those at the other regions. Input impedance of the circulator is shown in Fig. 3. The reference plane is chosen arbitrarily.

To identify those operation modes, resonance frequency dependence on length and diameter is determined. Results are shown in Fig. 4 for a 6-mm-diam ferrite post and in Fig. 5 for a 5.4-mm-diam ferrite post. The resonance frequencies are measured by measuring the input impedance as a function of frequency. Circled arrows

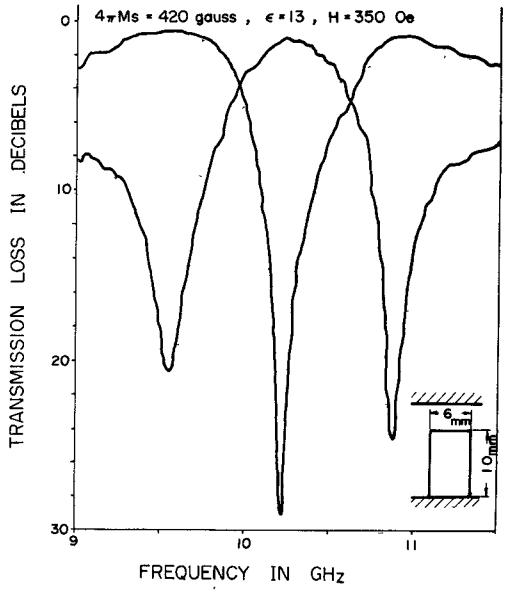

Fig. 2. Transmission losses of the circulator.

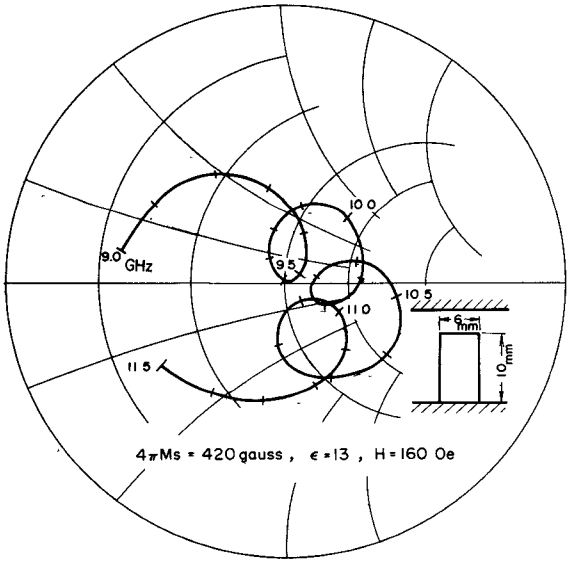

Fig. 3. Input impedance of the circulator.

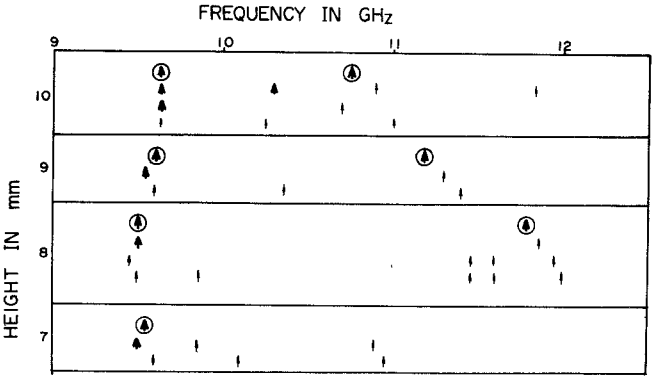

Fig. 4. Resonance frequencies obtained by measuring input impedance as a function of frequency. Ferrite post diameter is 6 mm. Circled arrows are for no applied dc magnetic field. Larger and smaller arrows represent overcoupled and undercoupled cases, respectively. For arrows in the same row, the same field is applied. The larger field is applied for the arrows in the lower row for the same ferrite dimensions.

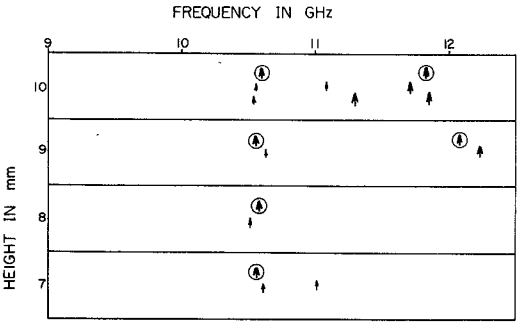

Fig. 5. Resonance frequencies obtained by measuring input impedance as a function of frequency. Ferrite post diameter is 5.4 mm. Figure explanations are the same as those in Fig. 4.

are for no dc applied field. The larger arrows represent overcoupled cases and the smaller arrows represent undercoupled cases. For arrows in the same row, the same field is applied. The mode for the middle operating region disappears as the applied field is diminished and as the ferrite post length becomes short. The modes which exist even when no field is applied, exist for any value of diameter and length. These modes are $HE_{11l}{}^{0\infty}$ as Owen [6] identified previously.

Measured resonance frequencies are compared with frequencies calculated by (16) in Table I. The frequency dependence on length and diameter are well explained by the TM-mode theory. The agreement between measured and calculated values is better for $HE_{111.5}{}^{0\infty}$ than for $HE_{110.5}{}^{0\infty}$.

TABLE I

COMPARISON OF MEASURED $HE_{11l}{}^{0\infty}$ MODE AND CALCULATED $TM_{11l}{}^{0\infty}$ MODE FREQUENCIES

l = 0.5

	D = 2R = 6 mm			D = 2R = 5.4 mm		
L mm	CAL (f)	MEA (f')	$\frac{f'-f}{f}$ ×100	CAL (f)	MEA (f')	$\frac{f'-f}{f}$ ×100
10	8.39	9.5	13 %	9.27	10.6	14 %
9	8.45	9.6	13	9.32	10.6	14
8	8.53	9.5	12	9.40	10.6	13
7	8.65	9.6	12	9.50	10.6	13

l = 1.5

	D = 2R = 6 mm			D = 2R = 5.4 mm		
L mm	CAL (f)	MEA (f')	$\frac{f'-f}{f}$ ×100	CAL (f)	MEA (f')	$\frac{f'-f}{f}$ ×100
10	10.25	10.75	4.9 %	10.96	11.8	7.7 %
9	10.68	11.2	4.7	11.38	12.1	6.1
8	11.26	11.8	4.4	11.93		
7	12.06			12.69		

Two neglected facts can be considered as reasons why the measured and calculated values are different: one is the disturbance of fields at the junction where the terminal waveguide mode changes to radial line modes and another is the assumed perfect open boundary conditions and therefore the assumption of a $TM_{111}^{0\infty}$ instead of an $HE_{111}^{0\infty}$ mode. In order to evaluate the effect of imperfect open boundary conditions, the TM_{110}^{00} mode is investigated. Calculated and measured [6] values are compared in Table II. The relative difference in frequency takes a large value of about 30 percent. Considering the imperfect open boundary conditions, resonance frequencies are recalculated [11] by (17). The result is shown by a solid line in Fig. 6. Measured values are shown by dots. The agreement is very good. The theoretical curve obtained by (16) is shown by a broken line. Thus it is shown that the major reason for the disagreement in calculated and measured resonance frequencies is the assumption of perfect open boundary conditions.

To identify the mode for the middle operating region in Fig. 2, eigenvalues are measured as a function of frequency after Owen [6]. Results are shown in Fig. 7. When the dc magnetic field is applied, the rotational phase eigenvalues split. However the inphase eigenvalue is affected only very little. It is seen from Fig. 7 that two, not three, resonances occur, causing phase rotation of 720°. One more resonance for the middle frequency operation region does not occur, even if the dc magnetic field is applied. Careful inspection shows that circulator operation is possible at the middle frequency operation region: phase separation between eigenvalues are 120°. The direction of circulation is also understood: the order of eigenvalue phase arrangement in the middle region is opposite to those in the side regions. The 240° separation between rotational phase eigenvalue at the middle region is due to the cooperative interference of the two resonance modes.

TABLE II
COMPARISON OF MEASURED [6] AND CALCULATED FREQUENCIES FOR TM_{110}^{00} MODE

$\ell = 0$			
D=2R mm	CAL (f)	MEA (f')	$\frac{f'-f}{f} \times 100$
5 1	9 5	11 6	22 %
5 6	8 6	10 8	25
6 1	7 9	10 1	28
6 6	7 3	9 6	32
7 1	6 8	9 0	32
7 6	6 4	8 4	34

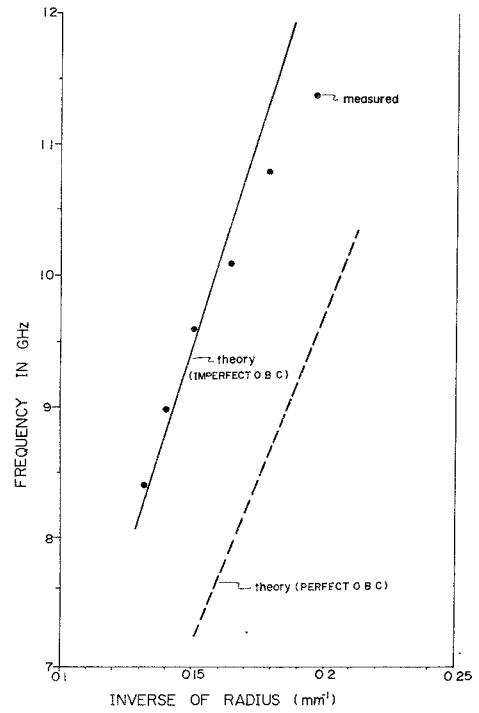

Fig. 6. Comparison of calculated and measured [6] resonance frequencies for TM_{110}^{00} mode.

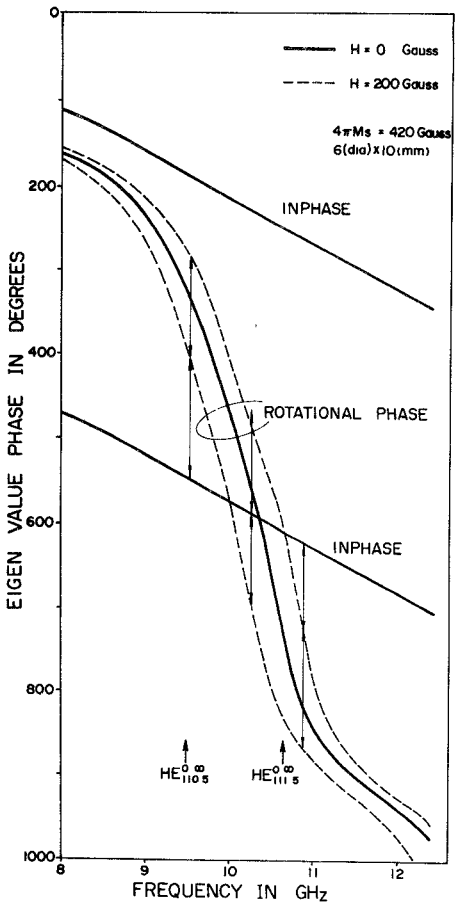

Fig. 7. Measured eigenvalue phases as a function of frequency. Reference plane is 11.5 mm distant from the junction center.

A method involving inserting dielectric spacers between the waveguide and a ferrite post has usually been adopted. For this case, the operation mode is clarified by Owen. In this short paper, the effects of the Teflon spacer on the circulator performance are investigated in more detail.

Transmission losses of the circulator with a 0.5-mm-thick Teflon spacer are shown in Fig. 8. Ferrite post dimensions are the same as those in Fig. 2. Input impedance of the circulator calculated from

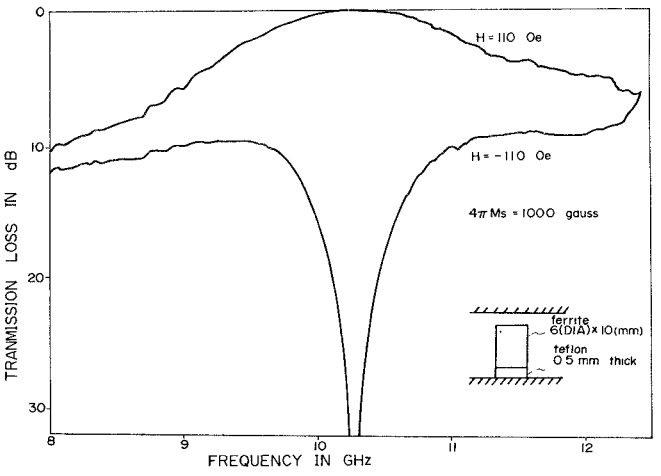

Fig. 8. Transmission losses of a circulator with a Teflon spacer-loaded ferrite post.

the measured eigenvalues is shown in Fig. 9. The locus closely represents that of the ideal resonator and, therefore, bandwidth enlargement with external resonators is more effective, compared with the case shown in Fig. 3. The effects of a Teflon spacer on the eigenvalues are shown in Fig. 10. Since the relative dielectric constant of Teflon is much smaller than that of ferrite, it can be considered that the open-circuit condition can be approximately satisfied. The operation

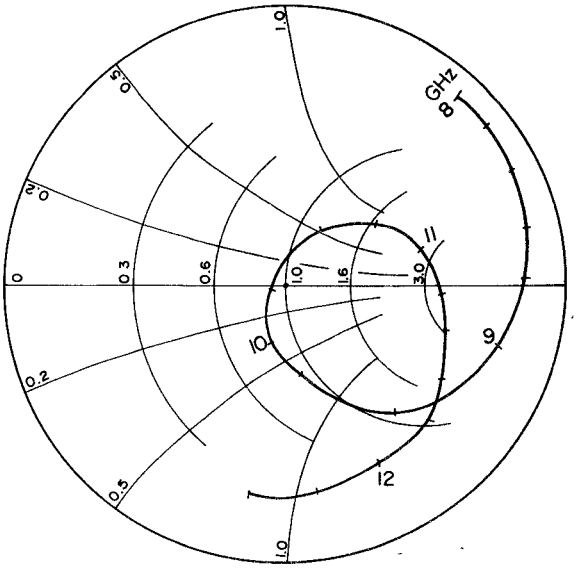

Fig. 9. Input impedance of a circulator with a Teflon spacer-loaded ferrite post calculated using the measured eigenvalues.

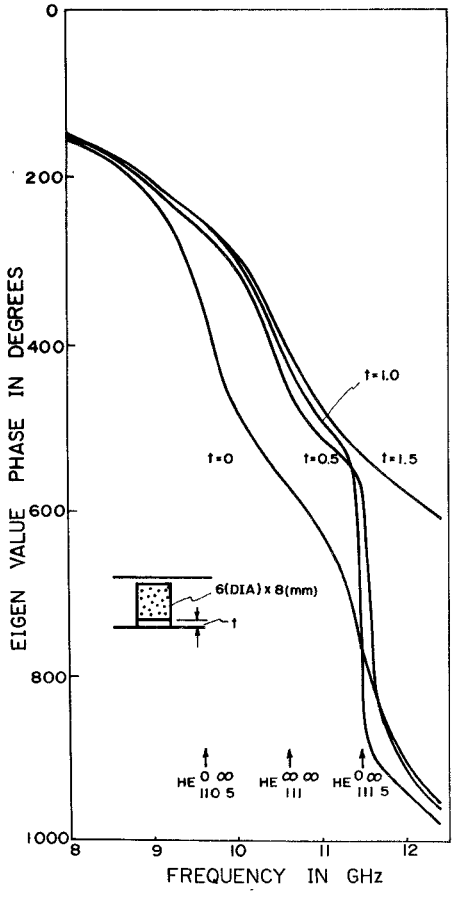

Fig. 10. Effects of a Teflon spacer on degenerated rotational phase eigenvalues.

TABLE III
COMPARISON OF MEASURED $HE_{111}^{\infty\infty}$ MODE AND CALCULATED $TE_{111}^{\infty\infty}$ MODE FREQUENCIES

	$l=1$			$l=2$
L_{mm}	CAL (f)	MEA (f)	$\frac{f'-f}{f}\times 100$	CAL
10	9 13	10 3	13	11 63
9	9 35	10 4	11	12 31
8	9 64	10 6	10	13 20

mode is $HE_{111}^{\infty\infty}$. Comparison of measured frequencies and frequencies calculated by (16) is made in Table III. Relative difference is about 10 percent. The frequency dependence on the ferrite post length is explained well.

The interval between resonance frequencies is more widespread for $HE_{mnl}^{\infty\infty}$ modes than $HE_{mnl}^{0\infty}$ modes. This is one of the reasons that dielectric spacers are usually employed.

The other resonance modes which have not been identified show a very little dip in input impedance locus and circulation never occurs at these mode frequencies.

IV. OPERATION MODES WITH A TRIANGULAR FERRITE POST

A triangular ferrite post has also been used in a waveguide Y circulator. Circulator construction is shown in Fig. 11. The operation of a circulator with a triangular ferrite post is so far understood only qualitatively where a broad-band matching effect is added to the operation with a circular ferrite post. Recently, it has been shown [13] that field analysis can be carried out for a triangular demagnetized ferrite post by applying the triangular metal waveguide field theory [14].

The fields and resonance frequency are rewritten briefly. Since there are dual boundary conditions at a metal surface and open-circuit boundary of a ferrite surface, fields in a triangular ferrite post can be determined from fields in a triangular metal waveguide by the duality concept [12]. To consider TM modes in the ferrite post, TE fields of the waveguide should be employed. Fields for TE modes in the waveguide have been solved as follows [14]:

$$H_z = \frac{\chi^2}{j\omega\mu}\psi \tag{23}$$

$$\psi = T(x,y)e^{ik_{lz}z} \tag{24}$$

$$\begin{aligned} T(x,y) = {} & \cos\left[\frac{2\pi}{3b}l\left(\frac{x}{2}+b\right)\right]\cos\frac{\sqrt{3}\pi(m-n)y}{9b} \\ & + \cos\left[\frac{2\pi}{3b}m\left(\frac{x}{2}+b\right)\right]\cos\frac{\sqrt{3}\pi(n-l)y}{9b} \\ & + \cos\left[\frac{2\pi}{3b}n\left(\frac{x}{2}+b\right)\right]\cos\frac{\sqrt{3}\pi(l-m)y}{9b} \end{aligned} \tag{25}$$

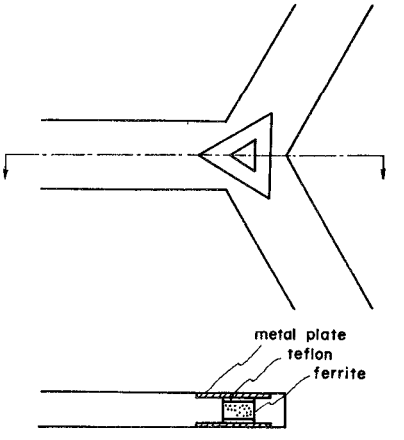

Fig. 11. Construction of a circulator with a triangular ferrite post.

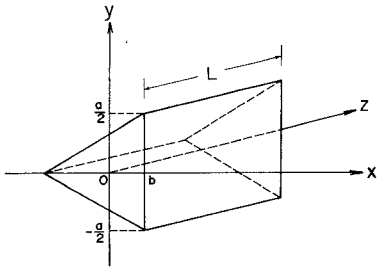

Fig. 12. Coordinates of a triangular ferrite post.

where l, m, and n are integers, never take zero value simultaneously, and must satisfy the following equation:

$$l + m + n = 0 \tag{26}$$

and where b is the radius of an inscribed circle of the triangle. The illustration of coordinates is shown in Fig. 12. The other fields are derived from H_z. Using the relations

$$\chi^2 = \left(\frac{4\pi}{3a}\right)^2 (m^2 + mn + n^2) \tag{27}$$

$$\frac{\partial^2\psi}{\partial x^2} + \frac{\partial^2\psi}{\partial y^2} + \frac{\partial^2\psi}{\partial z^2} = -\omega^2\epsilon\mu \tag{28}$$

$$\frac{\partial^2\psi}{\partial x^2} + \frac{\partial^2\psi}{\partial y^2} = -\chi^2\psi \tag{29}$$

resonance frequency is given as follows:

$$f = \frac{1}{2(\epsilon\mu)^{1/2}}\left[\left(\frac{4}{3a}\right)^2 (m^2 + mn + n^2) + \left(\frac{p}{L}\right)^2\right]^{1/2} \tag{30}$$

where a is the length of the sides of the triangle, i.e., $a = 2\sqrt{3}b$, and the integer p is the same as l in (13)–(15). Fields in the ferrite post are derived by the interchange $H \rightarrow -E$, $E \rightarrow H$, $\epsilon \rightarrow \mu$, $\mu \rightarrow \epsilon$. Resonance frequency never changes with the interchange. Modes are designated as $TM_{(l,m,n)p^{z_1,z_2}}$ for convenience.

When the ferrite anisotropy is small, fields in a magnetized ferrite are approximately given by the following equations as the previous case for a circular ferrite post:

$$H_x \doteqdot -\frac{\omega\epsilon}{(\omega^2\epsilon\mu - k_l^2)^2}\left\{\omega^2\epsilon\kappa\frac{\partial E_z}{\partial x} + j(\omega^2\epsilon\mu - k_l^2)\frac{\partial E_z}{\partial y}\right\} \tag{31}$$

$$H_y \doteqdot -\frac{\omega\epsilon}{(\omega^2\epsilon\mu - k_l^2)^2}\left\{\omega^2\epsilon\kappa\frac{\partial E_z}{\partial y} - j(\omega^2\epsilon\mu - k_l^2)\frac{\partial E_z}{\partial x}\right\} \tag{32}$$

$$H_z = 0 \tag{33}$$

$$E_x = -j\frac{k_l}{\omega\epsilon}H_y \tag{34}$$

$$E_y = j\frac{k_l}{\omega\epsilon}H_x \tag{35}$$

where E_z is given from (23) by the interchange.

A comparison between frequencies calculated by (30), assuming $TM_{(1-10)1}^{\infty\infty}$ mode, and measured center frequencies of Y circulators developed by Nippon Electric Company are shown in Fig. 13. Measured frequencies fall fairly well on a straight line, as the theory predicts, although they are about 20 percent higher than calculated values. To obtain theoretically more precise frequency, the imperfect open boundary conditions should be considered.

A sketch of the field pattern is shown in Fig. 14. The field pattern rotates to the rotational phase eigen excitations. It is seen that circularly rotating magnetic fields are generated at the central part of the triangle.

V. CONCLUSION

Fields in a circular and a triangular ferrite post are solved taking into consideration the variation along the ferrite axis. Measured HE mode operation frequencies nearly agree with the calculated

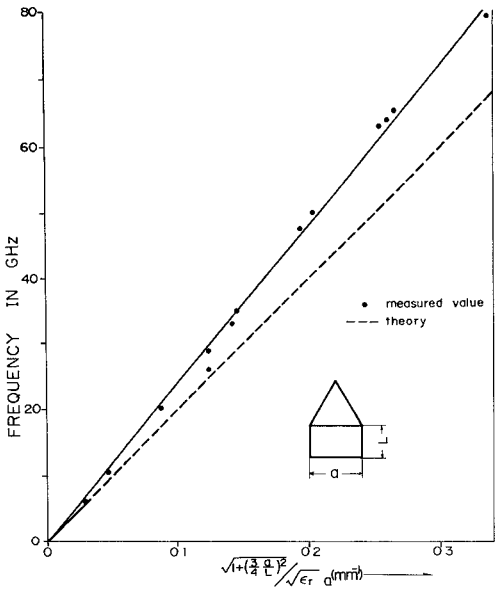

Fig. 13. Comparison of measured center frequencies and calculated resonance frequencies assuming a TM mode.

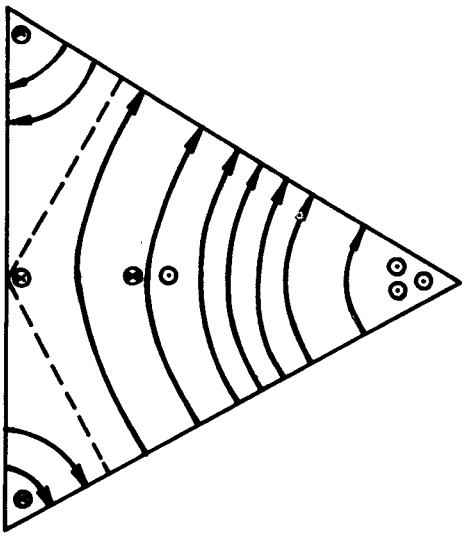

Fig. 14. Sketch of fields pattern for TM $_{(1-10)}$ mode. Solid lines represent magnetic field. Broken lines represent null magnetic field.

frequencies obtained by assuming a TM mode and perfect open-circuited boundary conditions. It is shown that the circulation occurs at the frequencies where two HE modes interfere with each other, besides occurring at HE mode resonance frequencies.

ACKNOWLEDGMENT

The author wishes to thank E. Kurosawa for his help in the experiments, Prof. N. Ogasawara for referencing his unpublished paper, Associate Prof. Y. Kobayashi and M. Yada for helpful discussion, and Y. Kasuga for supplying the waveguide Y-circulator data. He also wishes to thank Dr. H. Kaneko and Dr. M. Sugiyama for their encouragement and guidance.

REFERENCES

[1] H. N. Chait, and T. R. Curry, "Y circulator," *J. Appl. Phys.*, vol. 30, pp. 152–153, Apr. 1959.
[2] B. A. Auld, "The synthesis of symmetrical waveguide circulators," *IRE Trans. Microwave Theory Tech.*, vol. MTT-7, pp. 238–246, Apr. 1959.
[3] H. Bosma, "On stripline Y-circulation at UHF," *IEEE Trans. Microwave Theory Tech.*, vol. MTT-12, pp. 61–72, Jan. 1964.
[4] C. E. Fay and R. L. Comstock, "Operation of the ferrite junction circulator," *IEEE Trans. Microwave Theory Tech. (1964 Symposium Issue)*, vol. MTT-13, pp. 15–27, Jan. 1965.

[5] E. N. Skomal, "Theory of operation of a 3-port Y-junction ferrite circulator," *IEEE Trans. Microwave Theory Tech.*, vol. MTT-11, pp. 117–122, Mar. 1963.
[6] B. Owen, "The identification of modal resonances in ferrite loaded waveguide Y-junctions and their adjustment for circulation," *Bell Syst. Tech. J.*, vol. 51, pp. 595–627, Mar. 1972.
[7] J. B. Davies, "An analysis of the m-port symmetrical H-plane waveguide junction with central ferrite post," *IRE Trans. Microwave Theory Tech.*, vol. MTT-10, pp. 596–604, Nov. 1962.
[8] N. Tsukamoto, M. Suzuki, and T. Matsumoto, "An analysis of the waveguide Y-junction with ferrite," *Trans. Inst. Electron. Commun. Eng. Jap.*, vol. 54-B, pp. 131–138, Apr. 1971.
[9] S. Nakahara and H. Kurebayashi, "Circulator performance improvement by scattering matrix method," Paper Tech. Group on Microwaves, Inst. Electron. Commun. Eng. Jap., Dec. 1963.
[10] K. K. Chow, "On the solution and field pattern of sylindrical and dielectric resonators," *IEEE Trans. Microwave Theory Tech.* (Corresp.), vol. MTT-14, p. 439, Sept. 1966.
[11] Y. Kobayashi, "The resonators applied on strip lines," Paper Tech. Group on Microwaves, Inst. Electron. Commun. Eng. Japan., Jan. 1971.
[12] R. F. Harrington, *Time-Harmonic Electromagnetic Fields*. New York: McGraw-Hill, 1961.
[13] N. Ogasawara and T. Noguchi, "Modes identification of a dielectric triangular post resonator," to be presented at the 1974 Nat. Conv. Institute of Electrical Engineers of Japan.
[14] S. A. Schelkunoff, *Electromagnetic Wave*. New York: Van Nostrand.

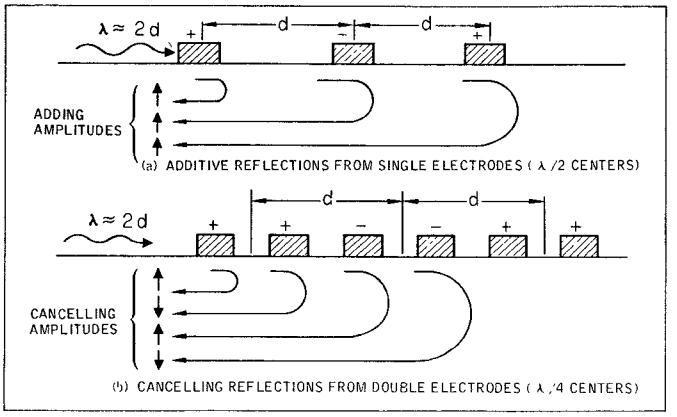

Fig. 1. Mass/electrical loading reflections of single and double electrodes.

Experimental Distinction Between Crossed-Field and In-Line Three-Port Circuit Models for Interdigital Transducers

W. RICHARD SMITH

***Abstract*—The crossed-field and in-line Mason circuit models for interdigital surface-wave transducers give opposite predictions for the dependence of acoustic reflection coefficients on electric load resistance for purely resistive loads. Experiments described herein show that the crossed-field model correctly describes the reflections for YX quartz, ST-X quartz, and YZ lithium niobate substrates. A low-resistance load minimizes reflections for transducers with double electrodes operating at the fundamental synchronous frequency. For single electrode transducers, optimum reflection suppression may call for a load resistance comparable to the transducer impedance.**

I. INTRODUCTION

The crossed-field and in-line three-port Mason circuits [1] for bulk-wave transducers have found wide usage as approximate equivalent circuits for interdigital surface-wave transducers [2]. Arguments for preferring both the in-line and crossed-field models have been suggested by various authors [3]–[6]. In addition, an intermediate mixed model has been proposed by Milsom and Redwood [7]. In [8] some differences between the models are emphasized, and it is stated that the choice of model apparently depends on the piezoelectric substrate.

This short paper provides an experimental basis for determining which model gives the better representation of a particular interdigital transducer and piezoelectric substrate. In addition, it negates a statement made earlier in [8] to the effect that the two models predict identical results for *all* transducer three-port transfer properties in the weak-coupling limit. The new finding reported here is that measurements of transducer acoustic reflection coefficients as a function of electric load resistance can determine which model is applicable, since the two models predict opposite behavior for purely resistive loads. Specific results are given in the following for "double electrode" [9] transducers on YX quartz, ST-X quartz, and YZ lithium niobate, and for a "single electrode" transducer on YZ lithium niobate.

II. ACOUSTIC REFLECTIONS

The experimental distinction between the crossed-field and in-line Mason circuits is based on measuring the acoustic reflection coefficient of a transducer as a function of the electric load. We begin by distinguishing the two causes of surface-wave reflections in interdigital transducers.

The first cause is the fact that metal electrodes short out the tangential electric field at the crystal surface and introduce mechanical loading, so that the electrode and gap regions have different apparent wave impedances [10], [11]. The second cause is that forward and backward surface waves are "regenerated" in the transducer by the voltage that the incident surface wave delivers to the electric load. The magnitude of the regenerated surface waves can be reduced (at a sacrifice in insertion loss) by varying the load impedance.

In ordinary single electrode transducers [Fig. 1(a)], the "mass/electrical loading" (MEL) reflections can become particularly troublesome because the metal stripes are spaced by one-half wavelength, causing MEL reflections to add in phase. The double electrode geometry [9] [Fig. 1(b)] provides a high degree of cancellation of the MEL reflections from successive electrodes, so that the reflections in double electrode devices are almost entirely of the regenerated wave (RW) type. Our purpose here is to determine a transducer circuit model which accurately describes the total (MEL and RW) reflections with particular emphasis on their relation to the electric load.

III. MASON CIRCUIT MODELS

The Mason circuits for bulk-wave transducers have found wide usage in surface-wave work since they give a three-port description of interdigital transducers, either periodic or dispersive with many nonidentical electrodes. In order to account for the different acoustic-wave impedances of the electrode and gap regions, the circuit of Fig. 2 has been used by at least two authors [10], [11]. In this circuit the unit cell of length d is subdivided into a metallized and an unmetallized region, with wave impedances Z_m and Z_0 in the corresponding acoustic transmission lines.

Synchronous operation is defined by the condition that d be equal to one-half acoustic wavelength ($\lambda = 2d$), and the circuit of Fig. 2

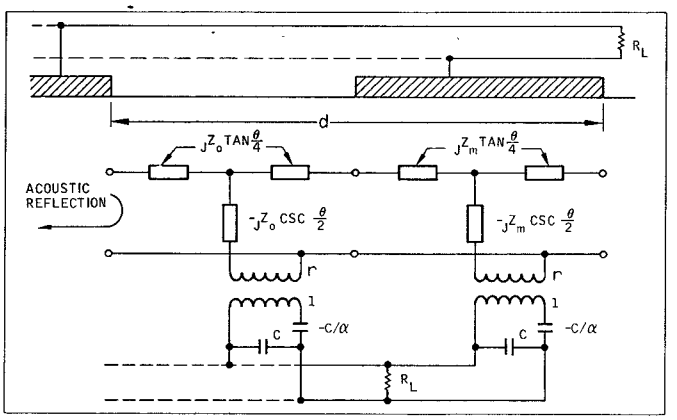

Fig. 2. Mason circuit model for single electrodes, including an acoustic-wave impedance discontinuity.

Manuscript received March 13, 1974; revised June 13, 1974. This work was sponsored by the U. S. Army Electronics Command, Fort Monmouth, N. J., under Contract DAAB07-73-C-0175.
The author is with Hughes Aircraft Company, Fullerton, Calif. 92634.